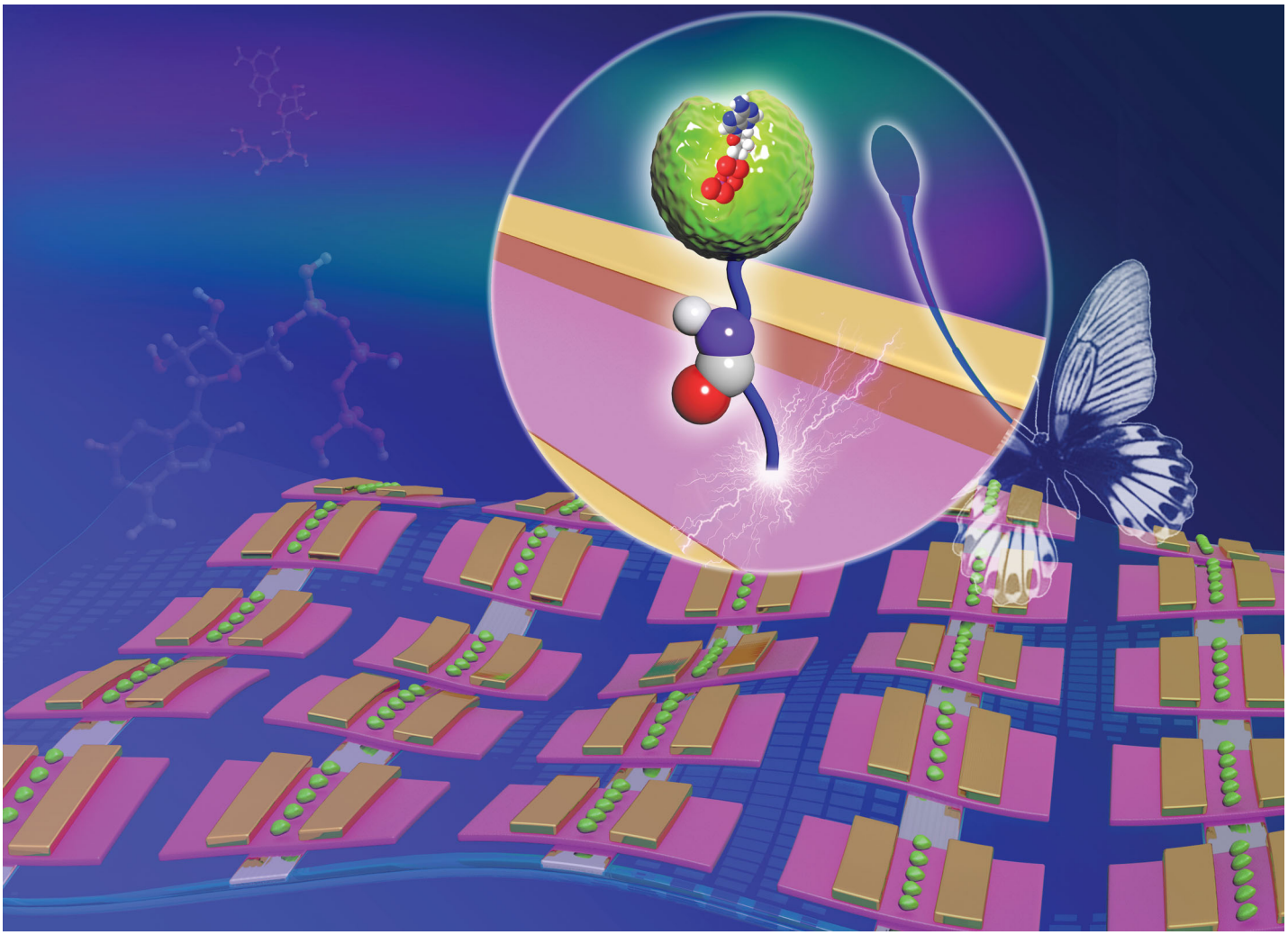

Showcasing research from Chong-an Di, Daoben Zhu and co-workers at the Institute of Chemistry, Chinese Academy of Sciences, Beijing

Molecular antenna tailored organic thin-film transistors for sensing application

By tailoring the neighboring-conductive-channel organic layer using a plasma-assisted-interfacial-grafting method, we introduced a molecular antenna on the surface of organic transistors to enable direct interaction between the semiconductors in the conductive channel and the target biological analytes in solution.

As featured in:

See Chong-an Di, Daoben Zhu *et al.*, *Mater. Horiz.*, 2018, **5**, 240.

ROYAL SOCIETY OF CHEMISTRY

rsc.li/materials-horizons

Registered charity number: 207890

Materials Horizons

COMMUNICATION

View Article Online
View Journal | View Issue

Cite this: *Mater. Horiz.*, 2018, 5, 240

Received 26th October 2017,
Accepted 19th December 2017

DOI: 10.1039/c7mh00887b

rsc.li/materials-horizons

Molecular antenna tailored organic thin-film transistors for sensing application†

Hongguang Shen,[ab] Ye Zou,[a] Yaping Zang,[ab] Dazhen Huang,[ab] Wenlong Jin,[ab] Chong-an Di *[a] and Daoben Zhu *[a]

By tailoring the neighboring-conductive-channel organic layer using a plasma-assisted-interfacial-grafting method, we introduced a molecular antenna onto the surface of organic transistors to enable direct interaction between the semiconductors in the conductive channel and the target analytes in solution. The specific interaction provides the OTFT with sensitive adenosine triphosphate (ATP) detection ability, which represents a step forward toward low-cost, flexible, and high throughput organic electronic biosensors.

Conceptual insights

Endowing organic thin-film transistors (OTFTs) with biosensing functions can open up novel opportunities for flexible and low-cost bioelectronic devices. To meet this critical requirement, the construction of OTFTs with well-designed biological–electronic interfaces is highly desired, but remains a challenge. We introduced a molecular antenna onto the surface of OTFTs by tailoring the neighbouring-conductive-channel organic layer using an *in situ* plasma-assisted-interfacial-grafting method. The functionalized interface can enable direct interaction between the semiconductors in the conductive channel and the target analytes in solution, which allows the detection of ATP with prominent selectivity, good reproducibility, and a low detection limit of 0.1 nM. More importantly, the sensing device can be built in a flexible array for high throughput biosensing application and even powered by commercial batteries. These excellent sensing properties make the molecular-tailored OTFTs a powerful platform toward portable and wearable medical diagnostic elements.

Introduction

Motivated by the urgent demand for advanced environmental monitoring and real-time healthcare diagnostic devices, the development of low-cost and flexible electronic sensors has attracted tremendous interest.[1–7] Organic thin-film transistors (OTFTs) offer a unique sensing platform by combining signal transduction and amplification to enable tunable sensing ability while maintaining a high signal-to-noise ratio.[8–10] More importantly, their compatibility with biosystems and solution-processing techniques make OTFTs theoretically suitable for low-cost bioelectronic applications.[1,11] Benefiting from these features and recent developments in functional OTFTs, the effective detection of biological species including DNA sequences and antibodies has been realized.[12–16] Despite these achievements, the construction of novel sensitive and selective OTFT-based biosensors is still highly desired, due to the limitation associated with weak and non-specific molecular interactions between semiconductors in the conductive channel and biological analytes in solutions.[17,18]

The introduction of bio-species onto the surface of the functional layer in the OTFT can serve as a general strategy to partly overcome the aforementioned issue. Till now, surface modification of both the organic semiconductor layer and the gate electrode has been utilized to fabricate selective bio-sensing devices.[1,7] As an example, Lai *et al.* and Minamiki *et al.* developed organic transistors with gate electrodes functionalized by complementary DNA probes and streptavidins for the selective detection of DNA or antibodies.[14,19] Interestingly, these kinds of devices possess good stability in solutions since the organic semiconductors are encapsulated by a dielectric layer. In spite of this advantage, the separate nature of the conductive channel and analytes hinders the direct interactions needed for prominent sensing performance.

The molecular design of organic semiconductors incorporating bio-functional groups is considered to be a straightforward strategy to enable an inherent semiconductor–analyte interaction.[20,21] However, the introduced bio-functional groups usually trap carriers, leading to a relatively low signal amplification ratio and sensing performance. The realization of prominent OTFT-based biosensors thus relies on the construction of devices with both high mobility and well-designed biological–electronic interfaces to bridge the gap between semiconductors and biological species.[1] Typical approaches to build bio-functional interfaces

[a] *Beijing National Laboratory for Molecular Sciences, CAS Key Laboratory of Organic Solids, Institute of Chemistry, Chinese Academy of Sciences, Beijing 100190, P. R. China. E-mail: dicha@iccas.ac.cn, zhudb@iccas.ac.cn*
[b] *University of Chinese Academy of Sciences, Beijing 100049, P. R. China*
† Electronic supplementary information (ESI) available. See DOI: 10.1039/c7mh00887b

in OTFTs have focused on the deposition of binding sites on the surface of organic semiconductors followed by the covalent immobilization of receptors. As representative examples, Bao *et al.* and Knoll *et al.* have recently put forward a series of binding sites, such as maleic anhydride (ppMa) and gold nanoparticles, for immobilization onto the surfaces of organic semiconductors. This therefore allows the covalent attachment of different receptors for the sensitive detection of DNA and proteins.[12,13,22] In spite of these exciting achievements, further enhancement of the interaction is limited by the sandwiched "molecular gap" between the surface semiconductor layer and the conductive channel (1–3 layers) located at the dielectric/organic layer interface,[23,24] and the "interaction boundary" between the surface molecular layer and the receptor separated by the binding sites. This makes the construction of OTFTs with well-located and high quality biological–electronic interfaces a key issue for state-of-the-art biosensors.

The *in situ* molecular tailoring of the neighboring-conductive-channel layer (NCCL) can, in principal, minimize the aforementioned molecular gap and enhance the semiconductor–receptor interaction, while maintaining efficient charge transport properties. This fine-tailoring strategy, however, can be hardly utilized to fabricate prominent OTFT-based biosensors because most organic films cannot survive the conventional chemical modification processes. Herein, we demonstrate OTFTs with a group-tailored NCCL by using a plasma-assisted *in situ* micro-damage interfacial grafting (PIMIG) approach. The chemically modified NCCL, together with the immobilized receptors, function as the sensing antenna for the devices. It therefore contributes to the selective detection of ATP with a low detection limit of 0.1 nM, and allows for high throughput low-voltage detection under bending conditions. The results demonstrate promising applications of molecular-antenna-tailored OTFTs as portable biosensors.

Bottom-gate top-contact OTFTs were fabricated using a conventional method (see the ESI†). The diketopyrrolopyrrole (DPP)-based polymer, poly-(diketopyrrolopyrrole-terthiophene) (PDPP3T), was selected as the organic semiconductor owing to its prominent performance in different OTFT applications.[25–28] A few PDPP3T layers and a tailored NCCL were functionalized as the conductive channel and the sensing antenna, respectively (Fig. 1a). Since the mobility reached a plateau at a minimum thickness of 8–10 nm (Fig. S1, ESI†) and 1–2 molecular layers are required for *in situ* surface modification and receptor binding, the active layer thickness of the sensing devices is controlled to be 12 nm. 50 nm SiO_2 was utilized as the dielectric layer to ensure low voltage and stable operation in solutions. Pristine devices exhibit mobility in the range of 0.3–0.6 $cm^2\ V^{-1}\ s^{-1}$ and show clear FET characteristics with well-defined linear and saturation regimes (Fig. S2, ESI†).

The *in situ* surface modification of the NCCL with specific binding groups is a prerequisite for receptor implantation and also for the construction of the so-called molecular antenna. Plasma treatment was employed not only because of its ability to generate active groups,[29,30] but also because it relies on the etching of the semiconductor, which can be used to control the location of the functional interface. Fig. 2a shows the mobility of the fabricated OTFTs upon plasma treatment at different treatment powers and exposure times. It is worth noting that the conductive channel can be etched upon oxygen plasma treatments of high treatment power and long exposure time. As a result, mobility decreases upon increasing the treatment power from 24 to 48 W and increasing the exposure time from 1 to 4 min. When the treatment power is maintained at 48 W for 4 min, the device suffers a dramatic decrease in mobility from 0.5 to 0.06 $cm^2\ V^{-1}\ s^{-1}$. In comparison, plasma treatment with a power of 24 W only results in a slight decrease in

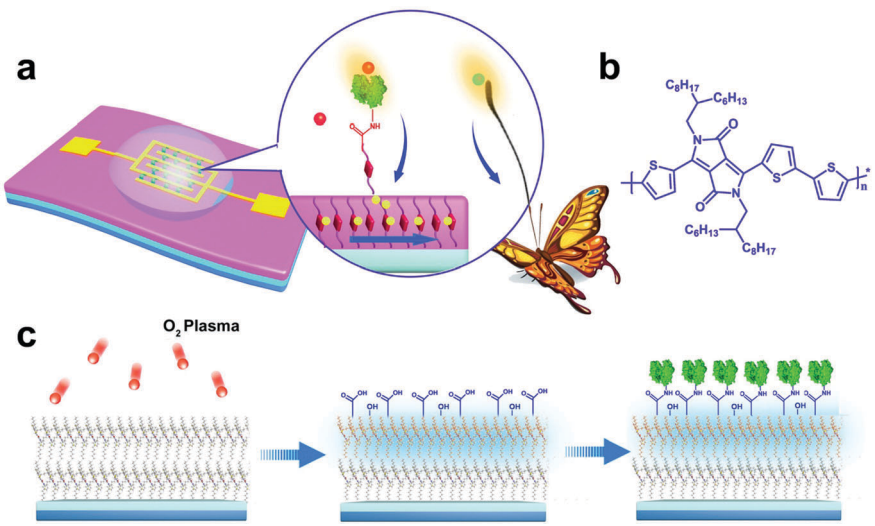

Fig. 1 (a) Schematic of an OTFT with a tailored molecular antenna for *in situ* bio-receptor grafting. The inset circle illustrates the molecular antenna of the modified device and a biological antenna of a butterfly. For the molecular antenna-tailored device, the receptor-modified semiconducting layer can bind with specific analytes to enable efficient and selective signal transduction. The signal recognition and signal transmission functionality are similar to the functions of a typical biological antenna. (b) The molecular structure of PDPP3T. (c) Schematic illustrations of the PIMIG approach to introduce binding groups and subsequently immobilize enzymes onto the surfaces of organic semiconductors.

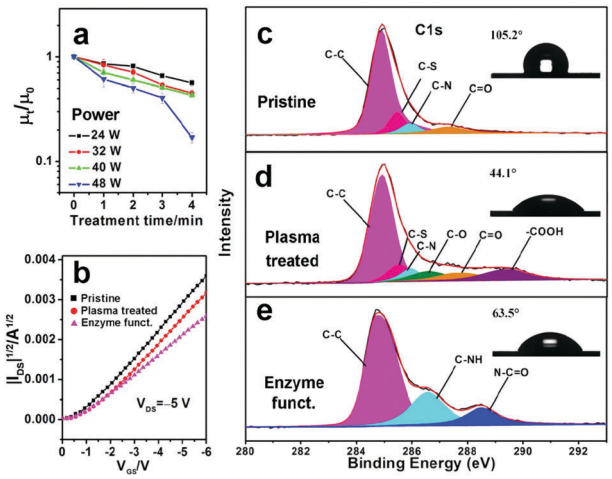

Fig. 2 (a) Relative mobility changes of the OTFTs upon O_2 plasma treatment at different treatment powers and exposure times. (b) Transfer curves for pristine, O_2 plasma treated (24 W, 2 min), and enzyme modified OTFTs. XPS spectra and static contact angle for (c) pristine, (d) O_2 plasma treated (24 W, 2 min), and (e) the enzyme immobilized PDPP3T film.

mobility with 60–90% of the initial performance retained, even after 4 min of treatment. It is worth noting that mobility over 0.4 $cm^2 V^{-1} s^{-1}$ can be consistently obtained when the exposure time is fixed at 2 min, which is the critical point to ensure both high device performance and well-located binding groups on the NCCL. More importantly, the approach is applicable for different organic semiconductors, such as pentacene and NDI(2OD)(4*t*BuPh)-DTYM2 (n-type) (Fig. S3, ESI†). These results clearly demonstrate that the fine-tuned plasma treatment can provide a simple but efficient approach to enable *in situ* interfacial modification of OTFTs.

X-ray photoelectron spectroscopy (XPS) characterization was performed to reveal the category of the functional groups generated by the plasma treatment. Fig. 2c and d show the XPS spectra of the pristine and plasma-treated films. The C 1s peak in the pristine film contains four components centered at 284.7, 285.3, 285.8, and 287.3 eV, corresponding to C–C, C–S, C–N, and C═O species, respectively. In the case of the plasma-treated film, both COOH (289.3 eV), C–O (286.5 eV) and shifted C═O (287.6 eV) groups can be identified (Fig. 2d). These results are consistent with plasma-induced surface oxidation. It should be noted that the intensity of the carboxyl peak (289.3 eV) increased when the power was enhanced from 8 to 24 W. However, a further increase in treatment power above 24 W results in no further increase in carboxyl intensity (Fig. S4, ESI†). This is consistent with the atomic force microscopy (AFM) results, indicating that obvious plasma-induced decreases in thickness occurred at a treatment power higher than 24 W (Fig. S5, ESI†) and this led to a significant decrease in mobility. Since the devices do not suffer from dramatic decreases in mobility with a treatment power of 24 W, the top 1–2 molecular layers of PDPP3T were tailored with binding groups. The phenomenon can be further supported by ultraviolet photoelectron spectroscopy (UPS) analysis, which shows the disappearance of the characteristic HOMO peak of PDPP3T, due to the disruption of the conjugated backbones of the surface layers (Fig. S6, ESI†). More importantly, the COOH group content of the treated surface reached 11.2%, which is higher than that of the C–O (8.2%) and C═O groups (8.7%). The high density of COOH groups on the PDPP3T surface, together with their high activity, can enable receptor immobilization, paving the way for various biosensing applications.

ATP, known as the "molecular unit of currency" for nearly all metabolic processes and an indicator used to evaluate neural activity, is considered as the direct energy source found in all forms of living organisms.[31–34] Therefore, the sensitive and specific detection of ATP is of great significance. To date, various transistor-type ATP sensing devices have been developed successfully. However, most of these devices are based on inorganic materials, such as silicon, carbon nanotubes, or even graphene.[35–39] OTFT-based ATP sensors are highly desired currently because they exhibit not only combined signal transduction and amplification, but also good flexibility for many wearable applications.[40] Here, we employed a commercialized hydrolytic enzyme, apyrase, as the receptor for ATP detection. In order to utilize the plasma-treated NCCL as the sensing molecular antenna, we covalently attached the enzymes onto the plasma treated semiconductors to enable specific interaction between organic semiconductors and analytes.

The successful biological functionalization process was characterized by XPS, AFM, and contact angle measurements. Upon the immobilization of enzymes, the emergence of peaks assigned to C–NH (286.2 eV) and O═C–NH (288.3 eV) groups was observed, indicating the covalent bonding of the enzymes (Fig. 2e). This is further verified by the AFM images (Fig. S7a, ESI†), since the treated PDPP3T layer is densely covered with nanoparticle-type structures (features of approximately 2–3 nm in height). Moreover, enzyme functionalization induces an increase in contact angle from 44.1° to 63.5° (Fig. 2d and e). Notably, both the XPS and AFM results suggest that enzyme modification was completed within one hour (Fig. S7 and S8, ESI†). Longer exposure time only results in physical absorption that can be easily removed by a typical cleaning procedure. As a result, the mono-enzyme-layer-modified NCCL can serve as the sensing antenna for PDPP3T-based OTFTs (Fig. S7d, ESI†).

The device performance of the modified OTFTs was characterized to evaluate its suitability for sensing application. As shown in Fig. 2b, the enzyme-functionalized OTFTs suffer from only slight changes in mobility upon modification, since mobilities of up to 0.33 $cm^2 V^{-1} s^{-1}$ (70% of the pristine value) can be obtained. The decrease in mobility should be attributed to the traps generated by the penetration of water or ions into the conductive channel during the aqueous modification process. It should be noted that a high on/off ratio ($\sim 10^3$) and low threshold voltage (V_{th}) (~ -1 V) were obtained when the device was operated in solution, where a fixed source–drain bias of −1 V was applied to avoid the electrolysis of electrolytes and the gate electrode.

To investigate the sensing performance of the molecular antenna-tailored OTFTs, I_{DS} was monitored upon addition of

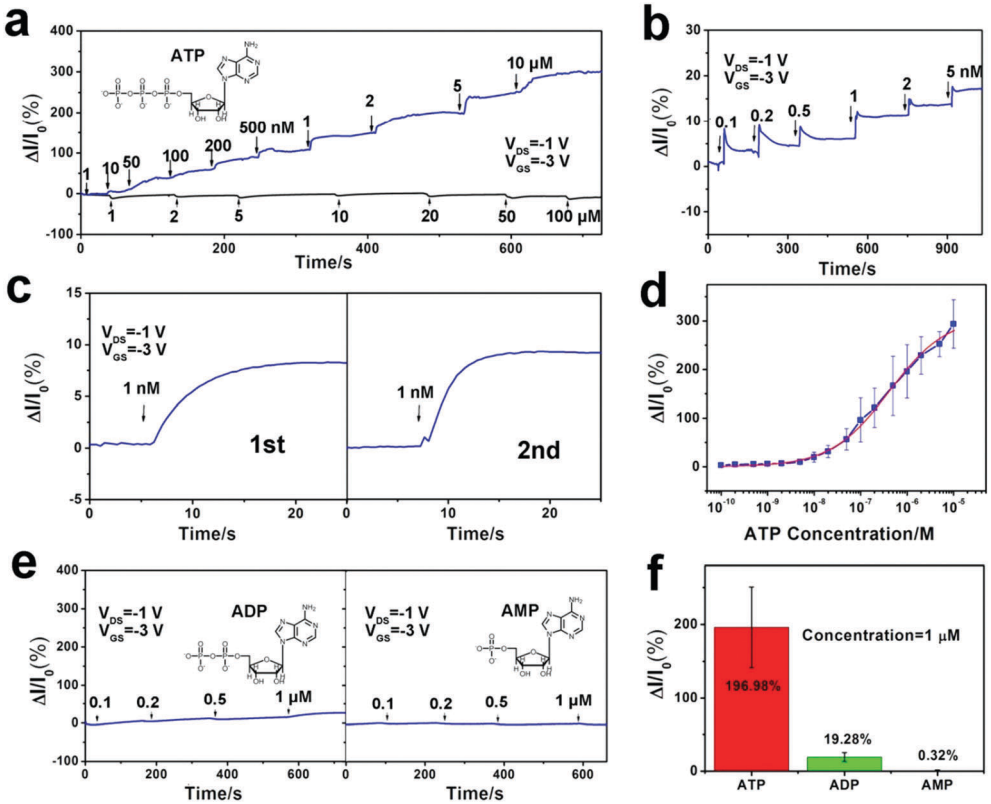

Fig. 3 Real-time I_{DS} response of an apyrase functionalized device upon exposure to ATP solution with concentrations ranging from (a) 1 nM to 10 μM (the blue line and the I_{DS} response of an untreated PDPP3T device to ATP is represented as the black line), and (b) 0.1 to 5 nM. (c) Reproducibility of $\Delta I/I_0$ of the sensing device to 1 nM ATP prior (left) and after (right) rinsing in pure sensing media. (d) Statistical $\Delta I/I_0$ *versus* ATP concentration for five devices. (e and f) Real-time $\Delta I/I_0$ of the device upon exposure to ATP, ADP, and AMP at a concentration of 1 μM.

ATP solutions at different concentrations in a buffered medium (HEPES, 0.1 mM, pH = 7.0). 5 mM $CaCl_2$ was added into the medium because Ca^{2+} activates the enzyme. Fig. 3a and b show the I_{DS} response upon exposure of the device to ATP. The I_{DS} response increases steadily with increasing ATP concentration from 0.1 nM to 10 μM. For example, 10 nM ATP resulted in an almost 20% increase in I_{DS}, while a remarkable increase in I_{DS} (~150%) was obtained at a concentration of 1 μM (Fig. 3a). In contrast, no obvious current changes were observed in the control experiments performed using devices without a molecular antenna or with an active layer thickness of over 20 nm (Fig. 3a and Fig. S9, ESI†). This thus indicates the critical role of the tailored NCCL in our sensing OTFTs. In particular, the detection limit of our devices was found to be 0.1 nM (Fig. 3b), which was about 15 times higher than the root-mean-square (RMS) of the noise level in $\Delta I/I_0$ (~0.2%) (the detection limit was defined as the critical point when the signal reached over three times the RMS[38]). Interestingly, it is six orders of magnitude lower than the previously published result (~100 μM) for an apyrase functionalized inorganic transistor,[35] and 10^2 times lower than a recently published nanometric OFET-based ATP biosensor.[38] A Langmuir–Hill isotherm model was utilized to fit the relationship between $\Delta I/I_0$ and ATP concentrations based on a statistic result (Fig. 3d). The result is consistent with that of an isothermal adsorption process similar to several previously published receptor-based transistor biosensors.[13,15,41,42] It is worth noting that I_{DS} increased linearly with the logarithm of ATP concentrations from 10 nM to 10 μM. The relative current change reached 75% per decade of ATP concentration. This excellent sensing performance makes the device suitable for the sensitive detection of bio-species in aqueous solutions.

Reproducibility and selectivity are important attributes for electronic sensors. To test the reproducibility of PDPP3T-based sensing devices, we studied the current response of the OTFTs upon repeated exposure to a solution containing a low concentration of ATP (1 nM). The device exhibited good reproducibility with comparable current response upon repeated exposure to the same solution (Fig. 3c). Moreover, adenosine diphosphate (ADP) and adenosine monophosphate (AMP), two analogues of ATP, were employed to probe the selectivity of the devices. As shown in Fig. 3e, the devices exhibited a much lower response to both ADP and AMP solutions in the concentration range of 0.1–1 μM. For example, 1 μM ATP brings on a large current change of 196.98%, while ADP and AMP at the same concentration only cause a small current response of lower than 20% (19.28% and 0.32%, respectively) (Fig. 3f). Since apyrase degrades ATP to ADP and successively to AMP with discriminative substrate selectivity to the three analytes,[35,43] a good ATP detection selectivity of the enzyme-modified sensing devices can therefore be achieved.

When the OTFTs operate in the linear regime, the current change of the devices at constant V_{DS} and V_{GS} can be written as:

$$\frac{\Delta I_{DS}}{I_{DS0}} = \frac{\Delta \sigma_{DS}}{\sigma_{DS0}} = \frac{\Delta N_h}{N_{h0}} + \frac{\Delta \mu_{lin}}{\mu_{lin0}} + \frac{\Delta N_h \Delta \mu_{lin}}{N_{h0} \mu_{lin0}} \quad (1)$$

where $\Delta\sigma/\sigma_0$, $\Delta N/N_0$ and $\Delta\mu/\mu_0$ are the relative changes in conductivity, carrier density and mobility, respectively, due to the recognition of ATP. Therefore, changes in the carrier concentration and mobility dominate the current response upon exposure to analytes. To identify the mechanism, the transfer curves before and after ATP exposure were measured (Fig. 4a). Notably, the introduction of 10 μM ATP leads to an obvious shift in V_{th} (~0.45 V) and a moderate increase in mobility (from 0.13 to 0.19 $cm^2\ V^{-1}\ s^{-1}$), implying that ATP exposure induces changes in both carrier concentration and mobility.

It is a well-known fact that protons can be generated during the ATP degradation process,[35,44] which can affect the charge transport behavior. To verify this mechanism, we measured the pH responses of the untreated PDPP3T devices (Fig. S10a, ESI†). The current was found to increase linearly when the pH values decreased from 7.0 to 4.0 (Fig. S10b, ESI†). The current change was further demonstrated by the transfer curves at different pH levels (Fig. 4c). The increased proton concentration leads to improved mobility and a slight shift in V_{th}. Since a much larger response to ATP (~300% for 10 μM) than that to a high concentration of protons (<100% at pH = 6.0, Fig. S10c (ESI†), the generated protons can be consumed when the pH level is lower than 6.0 due to the equilibrium of orthophosphate[35]) is observed, the proton sensing mechanism is not sufficient to account for the entire current response.

Given that the electrostatic interaction between the receptor and charged analyte is a fundamental process that can dominate signal transduction,[12,13,22,45,46] we propose two successive steps that are responsible for the detection of ATP (Fig. 4d). In the first step, the specific ATP–apyrase interaction induces the transfer of negative charge from ATP to the modified surface. It therefore induces positive charges in the channel *via* a field-effect mechanism and results in obvious changes in V_{th}.[47] In the second step, protons can be released during the ATP degradation process and they accumulate near the conductive channel owing to an applied gate field.[17] Interestingly, the accumulated protons can fill the traps in the conductive channel and contribute to the increase in mobility.

To validate the proposed first-step mechanism, sodium dodecyl sulfate (SDS) was utilized to introduce negative charges and thereby simulate the binding process of ATP. As expected, the addition of SDS leads to a positive shift of V_{th} while maintaining constant mobility in the enzyme-modified device (Fig. 4b), indicating that changes in the carrier concentration due to the field-effect induced positive charges in the channel region.[18,47,48] As a result, the functionalized devices display an obvious increase in I_{DS} upon exposure to SDS (Fig. S10d, ESI†), and achieved almost 230% in $\Delta I/I_0$. Since the introduction of negative charges only contributes to the variation in V_{th} rather than mobility, this confirms that the ATP detection results from a sensing mechanism involving two combined processes. More importantly, the distance between the conductive channel and the analytes in the solution dominates the field-effect-induced changes in the carrier concentration and trap-filling effect in the conductive channel.

The ultra-thin PDPP3T-based OTFT with a molecular antenna has two features that facilitate the sensitive and

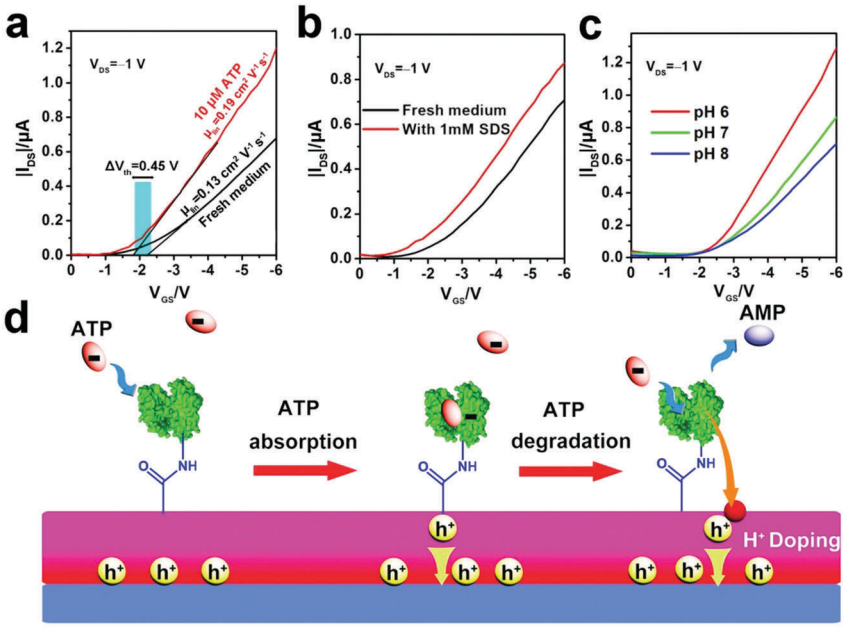

Fig. 4 Transfer curves of an apyrase functionalized device (a) operating in fresh medium and upon exposure to 10 μM ATP, (b) before and after exposure to 1 mM SDS. (c) Transfer curves of an untreated PDPP3T device upon exposure to a gradient pH-adjusted buffer solution. (d) Schematic illustration of the proposed sensing mechanisms of the ATP biosensor.

selective detection of ATP. First, the distance between the conductive channel and the analytes in the solution dominates the field-effect-induced changes in the carrier concentration and the trap-filling effect in the conductive channel. The molecular-antenna-tailored OTFTs can minimize the interaction distance and facilitate improvement in sensing performance. Secondly, the device-based PDPP3T possesses prominent device performance and stability even in solutions with a moderate proton level. It can thus ensure a high signal amplification ratio that results in excellent sensitivity.

In general, OTFTs for different sensing applications require the incorporation of various specific receptors. Therefore, tuning the molecular antenna is an important task. To assess the general applicability of the proposed device for different sensing applications, another commercial enzyme, catalase, was covalently immobilized onto the surface of PDPP3T for H_2O_2 detection. H_2O_2 sensors based on organic electrochemical transistors (OECTs) utilizing the intrinsic electrochemical activity of H_2O_2 have been reported with a detection limit ranging from 10 nM to 0.6 μM.[49–52] However, a ppb (~30 nM) level OTFT-based H_2O_2 sensor has not been achieved. Our catalase-tailored device displays excellent sensing performance with a Langmuir isotherm relationship between H_2O_2 concentration and the current response. A 70% decrease in I_{DS} can be obtained when the devices are exposed to 5 ppm H_2O_2, while the devices without a molecular antenna display only a slight increase in I_{DS} (10%) even at a higher concentration of 10 ppm. Interestingly, an effective detection of 1 ppb H_2O_2 was achieved with a fast response time of few seconds (Fig. S11, ESI†). This result indicates that the facile modulation of the molecular antenna in accordance with the needs of the desired sensing properties can be achieved.

Since OTFTs can be fabricated in large-area scale *via* solution processing techniques on different substrates, our devices hold considerable promise for low-cost flexible sensors. This advantage is particularly important for portable medical diagnostic sensors, which are often intended for high throughput parallel processing of multiple samples on the same chip. As a demonstration, we fabricated a 6 × 6 sensing matrix with an area of 8 × 8 cm^2 on a polyethylene terephthalate (PET) substrate (Fig. 5a). All the devices exhibited typical transistor behavior with mobility around 0.1 $cm^2\ V^{-1}\ s^{-1}$ and showed a prominent sensing ability at a V_{DS} and V_{GS} of −−1.0 and −−3.0 V, respectively (Fig. S12 and S13a, ESI†). By virtue of the low operating voltage, the flexible array can be driven by two commercial batteries (Fig. 5b and Fig. S13b, ESI†).

Fig. 5c shows the current responses of four devices. Similar to devices on silicon substrates, the four different OTFTs exhibit comparable current change upon exposure to ATP solutions with a fixed concentration of 1 nM, implying the real-time calibration ability of the sensing array. The calibrated devices can thus be utilized to achieve high-throughput detection of ATP at concentrations ranging from 1 nM to 1 μM (Fig. 5d and e). This is clearly demonstrated by the increase in $\Delta I/I_0$ from 1% at a concentration of 1 nM to 100% at 1 μM. Notably, the sensing array can operate at an operating voltage of 3 V under bending conditions, which is especially important for high throughput and flexible sensing applications.

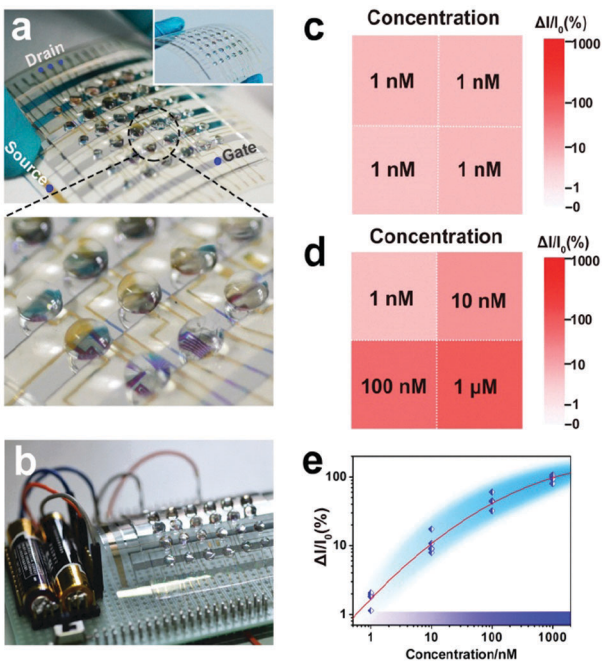

Fig. 5 Photograph of (a) a 6 × 6 sensing array on a flexible substrate and (b) battery-powered flexible sensing array. $\Delta I/I_0$ mapping of four devices upon exposure to ATP solutions with (c) a fixed concentration of 1 nM, and (d) varied concentrations from 1 nM to 1 μM. (e) $\Delta I/I_0$ upon increasing ATP concentration.

Conclusion

In conclusion, we report on OTFTs with a binding-group-tailored NCCL by employing a PIMIG approach. The modified surface enables the covalent immobilization of an enzyme that serves as a "molecular antenna", which can enable direct interaction between semiconductors in the conductive channel and the ATP in solution. The minimized molecular gap and decreased interaction boundary enhances the specific semiconductor–antenna–analyte interaction, leading to the selective detection of ATP with a low detection limit of 0.1 nM. More importantly, the prominent flexibility and good performance uniformity allows its successful application in flexible sensing arrays. Combined with the potential large-area production of flexible OTFTs and the general applicability of this method, the results emphasize the promising applications of OTFTs in portable medical diagnostic sensors.

Conflicts of interest

There are no conflicts to declare.

Acknowledgements

This research was financially supported by the National key R&D Program of China (2017YFA0204703), the Strategic Priority

Research Program of the Chinese Academy of Sciences (XDB12010000), and the National Natural Science Foundation (21422310, 61571423, 21643016).

Notes and references

1 D. T. Simon, E. O. Gabrielsson, K. Tybrandt and M. Berggren, *Chem. Rev.*, 2016, **116**, 13009–13041.
2 C. Liao, M. Zhang, M. Y. Yao, T. Hua, L. Li and F. Yan, *Adv. Mater.*, 2015, **27**, 7493–7527.
3 T. Someya, Z. Bao and G. G. Malliaras, *Nature*, 2016, **540**, 379–385.
4 G. Lanzani, *Nat. Mater.*, 2014, **13**, 775–776.
5 A. P. Turner, *Chem. Soc. Rev.*, 2013, **42**, 3184–3196.
6 J. Kirsch, C. Siltanen, Q. Zhou, A. Revzin and A. Simonian, *Chem. Soc. Rev.*, 2013, **42**, 8733–8768.
7 K. Manoli, M. Magliulo, M. Y. Mulla, M. Singh, L. Sabbatini, G. Palazzo and L. Torsi, *Angew. Chem., Int. Ed.*, 2015, **54**, 12562–12576.
8 Y. Zang, F. Zhang, D. Huang, C. A. Di, Q. Meng, X. Gao and D. Zhu, *Adv. Mater.*, 2014, **26**, 2862–2867.
9 W. Huang, X. Zhuang, F. S. Melkonyan, B. Wang, L. Zeng, G. Wang, S. Han, M. J. Bedzyk, J. Yu, T. J. Marks and A. Facchetti, *Adv. Mater.*, 2017, **29**, 1701706.
10 M. Berggren and A. Richter-Dahlfors, *Adv. Mater.*, 2007, **19**, 3201–3213.
11 D. Wang, V. Noël and B. Piro, *Electronics*, 2016, **5**, 9.
12 H. U. Khan, M. E. Roberts, O. Johnson, R. Forch, W. Knoll and Z. Bao, *Adv. Mater.*, 2010, **22**, 4452–4456.
13 H. U. Khan, J. Jang, J. J. Kim and W. Knoll, *J. Am. Chem. Soc.*, 2011, **133**, 2170–2176.
14 S. Lai, M. Demelas, G. Casula, P. Cosseddu, M. Barbaro and A. Bonfiglio, *Adv. Mater.*, 2013, **25**, 103–107.
15 M. Y. Mulla, E. Tuccori, M. Magliulo, G. Lattanzi, G. Palazzo, K. Persaud and L. Torsi, *Nat. Commun.*, 2015, **6**, 6010.
16 F. Buth, A. Donner, M. Sachsenhauser, M. Stutzmann and J. A. Garrido, *Adv. Mater.*, 2012, **24**, 4511–4517.
17 M. E. Roberts, S. C. Mannsfeld, N. Queralto, C. Reese, J. Locklin, W. Knoll and Z. Bao, *Proc. Natl. Acad. Sci. U. S. A.*, 2008, **105**, 12134–12139.
18 H. U. Khan, M. E. Roberts, W. Knoll and Z. Bao, *Chem. Mater.*, 2011, **23**, 1946–1953.
19 T. Minamiki, T. Minami, R. Kurita, O. Niwa, S.-I. Wakida, K. Fukuda, D. Kumaki and S. Tokito, *Appl. Phys. Lett.*, 2014, **104**, 243703.
20 L. Torsi, G. M. Farinola, F. Marinelli, M. C. Tanese, O. H. Omar, L. Valli, F. Babudri, F. Palmisano, P. G. Zambonin and F. Naso, *Nat. Mater.*, 2008, **7**, 412–417.
21 Y. Yang, G. Zhang, H. Luo, J. Yao, Z. Liu and D. Zhang, *ACS Appl. Mater. Interfaces*, 2016, **8**, 3635–3643.
22 M. L. Hammock, O. Knopfmacher, B. D. Naab, J. B. H. Tok and Z. Bao, *ACS Nano*, 2013, **7**, 3970–3980.
23 C.-a. Di, Y. Liu, G. Yu and D. Zhu, *Acc. Chem. Res.*, 2009, **42**, 1573–1583.
24 F. Zhang, X. Dai, W. Zhu, H. Chung and Y. Diao, *Adv. Mater.*, 2017, **29**, 1700411.
25 Q. Zhang, Y. Sun, W. Xu and D. Zhu, *Macromolecules*, 2014, **47**, 609–615.
26 B. Wang, T. P. Huynh, W. Wu, N. Hayek, T. T. Do, J. C. Cancilla, J. S. Torrecilla, M. M. Nahid, J. M. Colwell, O. M. Gazit, S. R. Puniredd, C. R. McNeill, P. Sonar and H. Haick, *Adv. Mater.*, 2016, **28**, 4012–4018.
27 Y. Zang, F. Zhang, D. Huang, X. Gao, C. A. Di and D. Zhu, *Nat. Commun.*, 2015, **6**, 6269.
28 Y. Zang, H. Shen, D. Huang, C.-A. Di and D. Zhu, *Adv. Mater.*, 2017, **29**, 1606088.
29 M. S. Mauter, Y. Wang, K. C. Okemgbo, C. O. Osuji, E. P. Giannelis and M. Elimelech, *ACS Appl. Mater. Interfaces*, 2011, **3**, 2861–2868.
30 K. S. Siow, L. Britcher, S. Kumar and H. J. Griesser, *Plasma Processes Polym.*, 2006, **3**, 392–418.
31 C. Ponnamperuma, C. Sagan and R. Mariner, *Nature*, 1963, **199**, 222–226.
32 N. X. Tritsch, E. Yi, J. E. Gale, E. Glowatzki and D. E. Bergles, *Nature*, 2007, **450**, 50–55.
33 Y. Pankratov, U. Lalo, A. Verkhratsky and R. A. North, *Pfluegers Arch.*, 2006, **452**, 589–597.
34 W. Qiang, H. Hu, L. Sun, H. Li and D. Xu, *Anal. Chem.*, 2015, **87**, 12190–12196.
35 S. Migita, K. Ozasa, T. Tanaka and T. Haruyama, *Anal. Sci.*, 2007, **23**, 45–48.
36 S. Mukherjee, X. Meshik, M. Choi, S. Farid, D. Datta, Y. Lan, S. Poduri, K. Sarkar, U. Baterdene, C.-E. Huang, Y. Y. Wang, P. Burke, M. Dutta and M. A. Stroscio, *IEEE Trans. NanoBiosci.*, 2015, **14**, 967–972.
37 Y. Huang, H. G. Sudibya, D. Fu, R. Xue, X. Dong, L.-J. Li and P. Chen, *Biosens. Bioelectron.*, 2009, **24**, 2716–2720.
38 Y. Zhang, J. Clausmeyer, B. Babakinejad, A. Lopez Cordoba, T. Ali, A. Shevchuk, Y. Takahashi, P. Novak, C. Edwards, M. Lab, S. Gopal, C. Chiappini, U. Anand, L. Magnani, R. C. Coombes, J. Gorelik, T. Matsue, W. Schuhmann, D. Klenerman, E. V. Sviderskaya and Y. Korchev, *ACS Nano*, 2016, **10**, 3214–3221.
39 E. Suaebah, T. Naramura, M. Myodo, M. Hasegawa, S. Shoji, J. J. Buendia and H. Kawarada, *Sensors*, 2017, **17**, 1686.
40 Y. Zang, D. Huang, C. A. Di and D. Zhu, *Adv. Mater.*, 2016, **28**, 4549–4555.
41 S. R. Ahn, J. H. An, H. S. Song, J. W. Park, S. H. Lee, J. H. Kim, J. Jang and T. H. Park, *ACS Nano*, 2016, **10**, 7287–7296.
42 C. H. Naylor, N. J. Kybert, C. Schneier, J. Xi, G. Romero, J. G. Saven, R. Liu and A. T. Johnson, *ACS Nano*, 2016, **10**, 6173–6179.
43 C. G. Del, J. Puente, M. A. Valenzuela, A. Traversocori and O. Cori, *Biochem. J.*, 1978, **167**, 525–529.
44 Y. N. Lee, K. Okumura, T. Iwata, K. Takahashi, T. Hattori, M. Ishida and K. Sawada, *Talanta*, 2016, **161**, 419–424.
45 M. Jang, H. Kim, S. Lee, H. W. Kim, J. K. Khedkar, Y. M. Rhee, I. Hwang, K. Kim and J. H. Oh, *Adv. Funct. Mater.*, 2015, **25**, 4882–4888.
46 W. Huang, K. Besar, R. LeCover, P. Dulloor, J. Sinha, J. F. Martínez Hardigree, C. Pick, J. Swavola, A. D. Everett, J. Frechette, M. Bevan and H. E. Katz, *Chem. Sci.*, 2014, **5**, 416–426.

47 H. Chen, S. Dong, M. Bai, N. Cheng, H. Wang, M. Li, H. Du, S. Hu, Y. Yang, T. Yang, F. Zhang, L. Gu, S. Meng, S. Hou and X. Guo, *Adv. Mater.*, 2015, **27**, 2113–2120.
48 O. Knopfmacher, M. L. Hammock, A. L. Appleton, G. Schwartz, J. Mei, T. Lei, J. Pei and Z. Bao, *Nat. Commun.*, 2014, **5**, 2954.
49 C. Liao and F. Yan, *Polym. Rev.*, 2013, **53**, 352–406.
50 C. Park, C. Lee and O. Kwon, *Polymers*, 2016, **8**, 249.
51 H. Tang, F. Yan, P. Lin, J. Xu and H. L. W. Chan, *Adv. Funct. Mater.*, 2011, **21**, 2264–2272.
52 L. Kergoat, B. Piro, D. T. Simon, M.-C. Pham, V. Noël and M. Berggren, *Adv. Mater.*, 2014, **26**, 5658–5664.